Optical property variations from a precursor (isoprene) to its atmospheric oxidation products

Yaling Zeng[a,b], Zhenxing Shen[a,b,*], Tian Zhang[a], Di Lu[a], Guohui Li[b], Yali Lei[a], Tian Feng[b],
Xin Wang[c], Yu Huang[b], Qian Zhang[a], Hongmei Xu[a], Qiyuan Wang[b], Junji Cao[b]

[a] Department of Environmental Sciences and Engineering, Xi'an Jiaotong University, Xi'an, 710049, China
[b] Key Lab of Aerosol Chemistry & Physics, SKLLQG, Institute of Earth Environment, Chinese Academy of Sciences, China
[c] Multiphase Chemistry Department, Max Planck Institute for Chemistry, Mainz, 55128, Germany

GRAPHICAL ABSTRACT
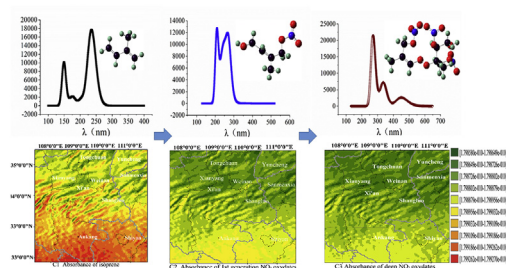
ARTICLE INFO

ABSTRACT

Isoprene is a crucial precursor of secondary organic aerosols (SOAs) that reacts with radicals or oxidants such as OH, O₃, and NO₃. The reaction mechanisms under various conditions have been elucidated through years of research. In this study, the UV–vis light absorptive ability of oxydates for isoprene was calculated at the PBE1PBE/6-311g (d) level using Gaussian 09. The results indicated that reactions of isoprene with OH and O₃ would produce less absorptive organics; the intensity of the absorption peaks and the maximum absorption wavelength decreased relative to those of the precursor. The oxydates formed from isoprene through an NO₃-initiated reaction had different light absorption properties. The optical properties of the oxydates exhibited a bathochromic shift and hyperchromic effect relative to those of the precursor. NO₃ mainly originated from vehicular traffic, indicating that anthropogenic activity heavily affected the formation of oxydates and light absorption. The light absorption properties and irradiation effect of SOAs caused by isoprene heavily depended on the reaction route. Transformation of functional groups was the dominated factor in photobleaching and photoenhancement of oxidative products. This study provides a detailed mechanism that explains the changes in optical absorption properties during isoprene oxidation.

1. Introduction

Secondary organic aerosols (SOAs) are critically linked to climate because of their ability to scatter and absorb radiation as well as to influence the number of cloud condensation nuclei (CCN)-sized particles through the formation of new particles or the growth of pre-existing particles (Moise et al., 2015). In general, biogenic volatile organic compound (BVOC) precursors dominate SOAs, with biogenic SOAs

comprising 90% of SOAs and anthropogenic secondary organic aerosols comprising 10% (Shrivastava et al., 2017). Among the hundreds of identified BVOCs, one compound dominates the annual global flux to the atmosphere: isoprene, which emitted from terrestrial and marine vegetation. Significant emissions of isoprene reinforce interrelated atmospheric phenomena such as radiative forcing and oxidant loss rate (Nguyen et al., 2016).

Oxidation of BVOC has been implicated as a potential source of condensable vapors or those involved in acidic multiphase chemistry (Inomata et al., 2014). In the troposphere, isoprene reacts frequently with hydroxyl radicals (OH), ozone (O_3), and nitrate radicals (NO_3), which are the leading factors for the transience of isoprene (Carlton et al., 2009). Because of its high concentration and reactivity with OH radicals, isoprene plays a crucial role in photochemistry within the atmospheric boundary layer (Bates et al., 2016). The reaction involving the OH radical is a major mechanism of oxidation during daytime (Mogensen et al., 2015). The OH-initiated reaction of isoprene was shown to lead to the formation of low-volatility species that condense to SOAs; this formation rate was as high as 3% (Kroll et al., 2006). Ozonolysis is a non-negligible part of isoprene transformation and global chemistry in the troposphere. Notably, the O_3 reaction occurs during both day and night. Because ozone is involved in many oxidation processes, ozonolysis of isoprene is a crucial part of the isoprene transformation mechanism (Inomata et al., 2014). The NO_3 radical and isoprene reaction was prevailed during the night (Horowitz et al., 2007). Nitrate radical chemistry can play a crucial role in isoprene transformation, but its effects on organic nitrate formation vary with the structure of the BVOC. A recent modeling study and other observations have reported that approximately 50% of total isoprene nitrate production occurs through the reaction of isoprene and NO_3 radicals (Horowitz et al., 2007). The kinetics and gas- and condensed-phase products of the reaction of isoprene with OH, O_3, and NO_3 have been the subject of experimental and theoretical studies for years. The reaction routes of these radical with isoprene are critical steps to atmospheric chemists; therefore, the first-, second-, and higher-generation products in various conditions have been elucidated (Inomata et al., 2014; Nguyen et al., 2016; Campuzanojost et al., 2004; Peeters et al., 2009; Schwantes et al., 2015).

A growing body of evidence suggests that some of the oxidates of isoprene, such as the light absorption components of brown carbon (BrC), undergo both photoenhancement and photobleaching during the formation process (Wong et al., 2017). Studies have illustrated the dynamic nature of BrC caused by oxidation processes, but the mechanisms leading to these observations remain unclear (Liu et al., 2016; Shen et al., 2017a; b). For example, whether all classes of compounds in BrC respond to photolytic oxidation in the same manner (e.g., initial photoenhancement followed by photobleaching) is unknown, as well as is whether different classes of compounds exhibit unique photolytic oxidation effects.

The wavelength-specific absorptivity of oxidates for BVOC depends on the precursors; while the formation pathways vary with the geographic location (Zhang et al., 2011). Molecular-level information on radical intermediates, as well as on gas- and particle-phase reaction products, is critical to gaining a realistic understanding of the light absorption properties of SOAs originating from isoprene reactions. Quantum chemistry calculation is an independent research method that has been a highly beneficial auxiliary approach for molecular-level research (Almandoz et al., 2014). In recent years, Gaussian 09 calculation has become a progressively effective method for theoretical studies on BVOC oxidation (Ignatov et al., 2014). The accuracy of time-dependent-density functional theory (TD-DFT) is mainly because of its more reliable description of electronic orbits compared with the Hartree–Fock method. In addition, TD-DFT has more advantages than Hartree–Fock method in dealing with electron correlation (Seibert et al., 2017).

Based on relevant literature, particular oxidation products formed

during the day (mainly through OH radicals and O_3) and at night (through O_3 and NO_3 radicals) are selected for analysis (Inomata et al., 2014). The following investigations were conducted: (1) the predominant reaction pathways of isoprene oxidized by OH, O_3, and NO_3 were determined, (2) UV–vis spectra of oxydates from the reaction of isoprene molecules were obtained using Gaussian 09, (3) changes in light absorption and radiative forcing were analyzed, and (4) the spatial distribution of the optical absorption property of the oxidized product was calculated in Guanzhong Basin (GZB), China as an example. The purpose of this manuscript was to give insight into the light absorption properties variations of oxidation products originating from the reactions of isoprene with OH, O_3, and NO_3.

2. Calculation methods

2.1. Quantum chemistry calculation

Quantum chemistry calculations based on Gaussian 09 have been applied in various fields and provides reliable results for theoretical studies (Ou et al., 2015). Theoretical UV–vis spectroscopy calculations using Gaussian 09 were originally applied to characterize the conjugated and aromatic structures of target molecules (Almandoz et al., 2014). The molecular structure of the ground state (GS) was optimized at the b3lyp/6-311g level with Gaussian 09 software on a Linux system. Based on obtained optimal structures, the UV–vis spectrum was calculated at the PBE1PBE/TZVP level (Ghosh et al., 2015).

Calculations of excited-state properties using TD-DFT have been used to obtain prevailing trends ever since the method was established (Doltsinis, 2014). The use of TD-DFT to calculate electronically excited states (EESs) has steadily increased over the past 20 years (Campetella et al., 2017; Ou et al., 2015). The energy difference between the EES and the GS determined at the GS geometry corresponds to an idealized (vertical) absorption:

$$E^{vert-abso} = E^{EES}(R^{GS}) - E^{GS}(R^{GS})$$

where $E^{vert-abso}$ $E^{vert-abso}$ is the energy gradient UV–vis spectrum computed from data in TD-DFT.

Calculations using the Perdew–Burke–Ernzerhof exchange correlation functional (PBE1PBE) (Ernzerhof and Scuseria, 1999) have strong performance in simulations of excited states (Huang et al., 2010).

Because calculation accuracy greatly depends on the basis set, we selected the high-level basis sets 6-311g (d) and TZVP for the calculations. The 6-311g (d) basis set can be a strong choice for relatively rapid yet meaningful calculations, whereas TZVP is a much larger basis set and could therefore rigorously describe molecular orbitals (Adamo and Jacquemin, 2013). These two basis sets are powerful tools that are widely used in various calculation methods (Ghosh et al., 2015; Peeters et al., 2014); several developments are further pushing them to the limit. New exchange–correlation functionals have been developed to calculate excited states, as well as double excitations and non-adiabatic effects (Adamo and Jacquemin, 2013).

2.2. WRF-chem numerical simulation

The regional near-ground level of isoprene was simulated using WRF-Chem 3.51. A specific version of the WRF-Chem model developed by Li et al. (2012) was utilized to investigate the formation of isoprene and its oxidized products in the GZB. The detailed description of GZB can be found in Feng et al. (2016). This version exploited a flexible gas-phase chemical module and the Community Multiscale Air Quality (version 4.6) aerosol module developed by the United States Environmental Protection Agency (Binkowski, 2003).

In this study, isoprene and its oxydates from April 12–25, 2013 were simulated. The time we selected was the first emission peak of isoprene which represented a typical distribution in GZB (Feng et al., 2016). The filter measurements of fine particular matter ($PM_{2.5}$), organic carbon

(OC), and elemental carbon (EC) were conducted in the GZB. The model was configured in a horizontal grid with a spacing of 3 km and 200 × 200 grid cells and centered at 34.25 N and 109 E. In the vertical direction, we used 35 levels in a stretched vertical grid with spacing ranging from 50 m (near the surface) to 500 m (at 2.5 km above ground level) to 1 km (above 14 km). The physics and dynamics of the configuration adopted the microphysics scheme of Hong and Lim, 2006, the Yonsei University planetary boundary layer scheme (Hong, 2006), the land surface scheme of five-layer thermal diffusion (Dudhia, 1996), the Dudhia shortwave scheme (Dudhia, 1989), and the rapid radiative transfer model long wave scheme (Mlawer et al., 1997). No cumulus parameterization was used because of the high horizontal resolution. GZB covers 50–70 grid cells and NCEP 1 × 1 reanalysis data were used for the meteorological initial and boundary conditions. In the present study, NCEP ADP Global Surface Observational Weather Data (http://rda.ucar.edu/) for the GZB were assimilated into the WRF-Chem model simulations using four-dimensional data assimilation to improve the simulation of the meteorological fields. The chemical initial and boundary conditions were interpolated from the model for ozone and the related chemical tracer (MOZART) output with a 6-h interval (Feng et al., 2016). The spin-up time for the simulation was 1 day. The MEGAN model was used to calculate the biogenic emissions in the model online (Guenther et al., 2012).

The model performance was validated using hourly ozone (O_3) and $PM_{2.5}$ observations at 13 monitoring sites in Xi'an and surrounding areas (released by the Ministry of Ecology and Environment, China) and the daily filter measurement of $PM_{2.5}$, EC, and OC at 29 sites in the GZB (Feng et al., 2016).

3. Results and discussion

3.1. Light absorption changes initiated by the OH radical during oxidation

OH-initiated oxidation of isoprene is a dominant route of formation of tropospheric SOAs (Lei et al., 2000). This reaction may be divided into three patterns according to the relative abundances of NO and OH (i.e., high NO and low OH, high OH and low NO, and low OH and low NO) (Shrivastava et al., 2017). We discussed each condition separately, and the reaction pathways were cross-verified with field study, laboratory experiment, and theoretical calculation results. Fig. S1 presents a simplified reaction schematic of the critical isoprene oxidation pathways initiated by the OH radical.

At high OH and low NO, OH-initiated reactions follow that O_2 can add to both the major OH-adducts either in the β-position or in the δ-position, resulting in β-OH-isoprenylperoxys (β-ISOPOOH) and σ-OH-isoprenylperoxys (σ-ISOPOOH) (Paulot et al., 2009). The second generation of ISOPOOH oxidized by OH produces isoprene epoxydiols (IEPOX); accordingly, the products have the isomers β-IEPOX and σ-IEPOX, which were denoted based on the position of the OH added. The products may be involved in further reactions (Paulot et al., 2009), which are not discussed in this paper. IEPOX appeared to be mostly low-volatility material, and the major products were in the particle phase (Peeters et al., 2014). The optical absorption properties of isoprene oxidation products were apparent in UV–vis spectrum by Gaussian 09 model calculation. The discrepancies between the original and the first- and second-generation products can be easily recognized in Fig. 1. The wavelengths of the maximum absorption peaks ($λ_{max}$) of isoprene, β-ISOPOOH, β-IEPOX, σ-ISOPOOH, and σ-IEPOX were 253.3, 167.5, 155.5, 219.4, and 154.4 nm, respectively; and their peak intensities, which was the indication of molar absorption coefficient ($ε$, epsilon), were 17693.94, 13027.61, 6854.62, 5737.53, and 6303.64, respectively. The β-path excitation energy decreased from 253.3 to 167.5 to 155.5 nm, and the oxidation degree further increased the excitation energy. The σ path decreased with the same tendency but through a different route. The wavelength shifted from the short-ultraviolet (SUV, 200–300 nm) region to the vacuum ultraviolet (VUV,

10–185 nm) region. The light absorption intensity dropped from isoprene to its oxidation products.

At high NO and low OH levels, the reaction between isoprene and NO form an alkoxy radical, which tends to fragment into products with higher volatility, including methacrolein (MACR) and methylvinyl ketone (MVK), isomerize to hydroxycarbonyl, or both (Bates et al., 2016; Campuzanojost et al., 2004). Because the fraction of hydroxy nitrate isomer species produced by the ISOPO₂/NO reaction was minor (approximately a 7% yield) (Lockwood et al., 2010), we do not further discuss the optical property of this species in this paper. The UV–vis spectrum of MACR and MVK can be seen in Fig. 1B; the $λ_{max}$ intensities at 209.8 and 209.2 nm were 12144.34 and 10623.23, respectively. The two structural isomers produced similar peak shapes at similar wavenumbers. The oxidation caused a slight blueshift of the $λ_{max}$, while the $λ_{max}$ of the isoprene was located in the SUV region.

When both OH and NO levels were low, two pathways followed the peroxy radical 1, 6-H shift to form photolabile hydroperoxy-methylbutanals (HPALDs) (Peeters et al., 2014); their optical properties are given in Fig. 1C. The wavelengths for HPALDs I and II were 165.1 and 220.9 nm, respectively, whereas their absorbance intensities were 6586.01 and 19417.19, respectively. Evidently, the wavelength oblueshifted because of varying degrees of oxidation. The peak intensity of HPALD II was higher than that of isoprene, whereas the opposite was true for HPALD I.

The aforementioned first and/or second comparative stable oxidized products had high molecular weights. Additionally, the second- and higher-generation oxidation products of isoprene were more likely to partition to the condensed phase than the first-generation products (Carlton et al., 2009). The absorption intensity and $λ_{max}$ generally decreased because of the hypochromic shift and hypochromic effect caused by the oxidation of isoprene by OH. The shift in the spectrum could be detected only by using a vacuum UV–vis spectrophotometer; the $λ_{max}$ was lower than 200 nm. Therefore, the oxidation process initiated by OH was a depressor of the radiative forcing of isoprene.

The conversion of excitation energy accounts for this phenomenon. The isoprene chromophore is a carbon–carbon double bond, which can lead to a π→π* transition when induced. Aldehydes, ketones, alcohols, and peroxyacid are chromophores of the oxidation products. These chromophores typically undergo n→σ* and n→π* transitions when excited. The higher excitation energy for the n→σ* transition compared with that of the π→π* transition accounted for the lower λ of the corresponding peak. Because of the low energy gap of the n→π* transition, its corresponding peaks were weak. Accordingly, the strongest peak of the oxidation products was induced by the n→σ* transition, which occurred in the far-ultraviolet region (FUV) region. Compared with the π→π* excitation peak, the n→σ* transition was hypochromic.

3.2. Changes in light absorption during the ozone-initiated reaction

Ozonolysis is an indispensable part of isoprene transformation in the troposphere (Inomata et al., 2014). Products of the reaction of isoprene with ozone have been studied through chamber reaction and filed observation (Nguyen et al., 2016). With many of the chemical constituents from the reaction is identified, the mechanism of isoprene ozonolysis is close to being completely understood (Ghosh et al., 2015). Identification of approximately 50% of the reacted isoprene, including MACR and MVK, was successful (Paulson and Seinfeld, 1992). Some crucial intermediates such as Criegee radicals, or significant effects such as H rearrangements, were used to establish the reaction mechanisms (Nguyen et al., 2016). The reaction pathways discussed in this paper (Fig. S2) were verified against field studies, laboratory research, and theory calculations (Inomata et al., 2014; Nguyen et al., 2016; Campuzanojost et al., 2004; Peeters et al., 2009; Schwantes et al., 2015). For convenience of description, the two reaction routes were named MVK and MACR routes; in the MVK route, the products of each step were named from OZ1 to OZ5, whereas in the MACR route, they
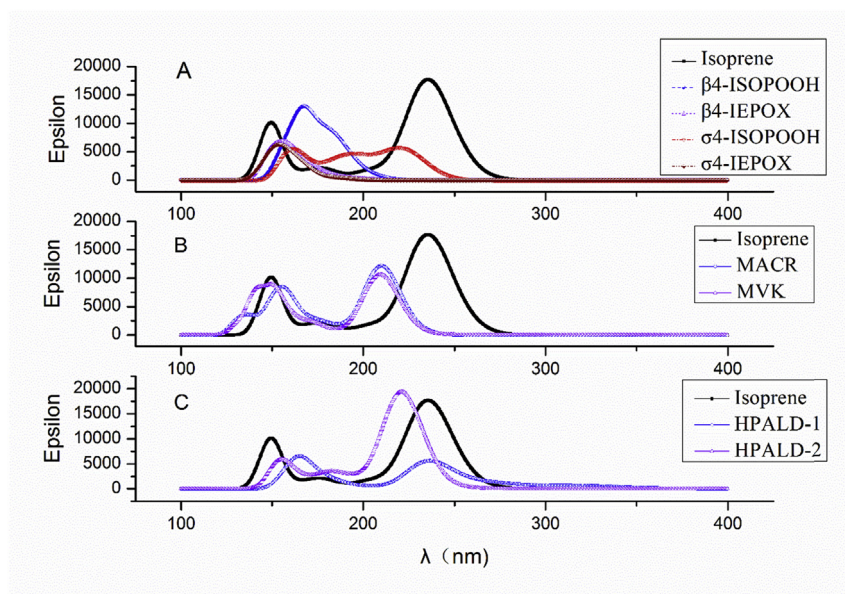
Fig. 1. UV–vis spectrum of the oxydates of isoprene reacted with OH.

were named from OZ6 to OZ10.

The first-generation carbonyl product of isoprene ozonolysis can react with ozone through a double bond. Ozone can bond to isoprene through addition; here, O_3 and α double bonds were the precursors of MACR, and the one bonded to γ was the precursor of MVK (Nguyen et al., 2016). When the addition had occurred, a stabilized Criegee intermediate (SCI) formed (Newland et al., 2015). Decarbonization transformed SCI to MACR and MVK by further ozonolysis, producing stable organic acids and esters.

The optical absorption variation during ozonolysis of isoprene was notable (Fig. 2). Both paths resulted in the slight shifting of peaks from the SUV to VUV regions. For the MARC route, λ_{max} changed from 253.3 to 179.2, 153.4, and 135.1 nm, finally reaching 136.3 or 154.3 nm when the two isomers formed; the maximum absorption peak (ε_{max}) values were 17693.94, 10205.639, 4538.095, 7736.74, 12206.068, and 9837.61, respectively. Similarly, the λ_{max} for the MVK route shifted from 253.3 to 169.2, 146.2, 146.5, 160.0, and 166.9; and the intensities

of peaks were 17693.94, 14078.12, 6792.46; 10613.67, 7213.49, and 10288.27, respectively. The general trend of wavelength and absorption intensity during ozonolysis was a decline, with minor variations between isomers (Fig. 2).

The chromophore carbonyl with the auxiliary functional auxochrome hydroxyl was behind the light absorption of the oxidation product. Carbonyl undergoes n→π* transition when excited, which is normally regarded as weak absorption. The hypochromic shift and hypochromic effect mechanism are evident in the analysis of the OH-initiated reaction, and both were highly similar. Therefore, the spectrum of the oxidation products suggests that the reaction with ozone leads to the hypochromic shift and hypochromic effect.

3.3. Changes in light absorption during the NO₃-initiated reaction

Isoprene/NO_3 chemistry is a mechanism of oxydative formation at night (Mogensen et al., 2015). NO_3 oxidation of isoprene typically
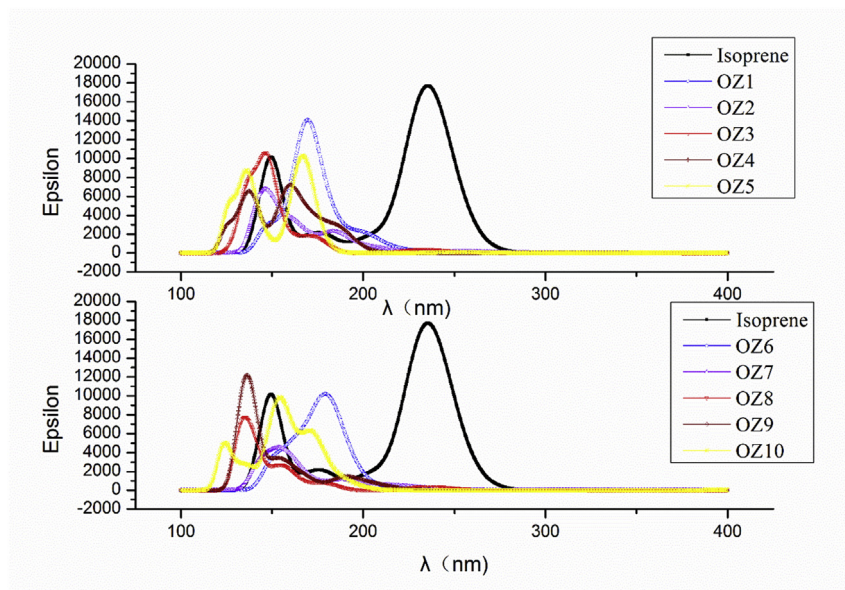
Fig. 2. UV–vis spectrum of the oxydates of isoprene reacted with O_3.

occurs at night because NO$_3$ readily undergoes photolysis under solar radiation (Schwantes et al., 2015). Because of its photolabile nature and rapid reaction with nitric oxide (NO), NO$_3$ is present primarily in the atmosphere at night. Oxidation products of nitrate radical chemistry have a unique chemical signature because of abundant sources. Organic nitrates (RONO$_2$), nitroxy organic acids, hydroxynitrates, nitroxy organic peroxides (e.g., nitroxyhydroxyperoxides), and nitroxy organosulfates have been detected by different laboratories and instruments (Horowitz et al., 2007; Suh et al., 2001; Schwantes et al., 2015). The reaction pathway we explored was verified against field studies, laboratory studies, and simulations. The paths chosen for analysis were those that produced the most abundant oxidation products. First-generation products with m/z ratios of 230, 232, and 248 were the major products (Ng et al., 2008; Schwantes et al., 2015). The established reaction mechanism was based on further reactions of the first-generation products. Although minor product ions at m/z ratios of 185, 377, and 393 were detected by Ng et al. (2008), we did not analyze the optical properties because of their tiny contribution. The oxidation products of isoprene were also found by chamber simulation and field study (Bates et al., 2016).

The reactions that provided the dominant products are presented in Fig. S3. The reactions proceeded by NO$_3$ addition to the C=C bond, forming four possible nitroxyalkyl radicals depending on the position of the NO$_3$ attack (Rollins et al., 2009). O$_2$ then oxidized the nitroxyalkyl radicals to two peroxy radicals (RO$_2$), which reacted further with HO$_2$, RO$_2$, or NO$_3$ radicals. The reaction of RO$_2$ and HO$_2$ radicals led to the formation of C5-nitroxyhydroperoxide (m/z 248). The reaction of the two RO$_2$ radicals (self- or cross-reaction) has three possible routes:

$$RO_2 + RO_2 \rightarrow 2RO + O_2 \quad (1a)$$

$$\rightarrow ROH + RCHO + O_2 \quad (1b)$$

$$\rightarrow ROOR + O_2 \quad (1c)$$
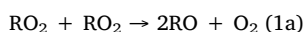
The second route results in the formation of C5-nitroxycarbonyl (m/z 230) and C5-hydroxynitrate (m/z 232). According to Equation (1b), these two products form at a 1:1 ratio; however, C5-nitroxycarbonyl could also be formed from alkoxy radicals (either from the RO$_2$/RO$_2$ or RO$_2$/NO$_3$ reactions). Observation of the first-generation gas-phase product C5-dinitrate was conducted using a chemical ionization mass spectrometer and electrospray ionization time-of-flight mass spectrometry (ESI-TOFMS) analysis (Surratt and Finlayson-Pitts, 2010). This first-generation gas-phase product was found previously by Werner et al. (1999). C5-nitroxycarbonyl (m/z 230) was the most abundant gas-phase product, and its further oxidation yielded product at MW 240 through the reaction with NO$_3$ or O$_3$ and with RO$_2$. Of all the observed products, the ion at m/z 232 appeared to be the most reactive with NO$_3$ radicals (Lin et al., 2013). It should be noted that we did not detect products from the further oxidation of C5-nitroxyhydroperoxide (m/z 248) (Surratt and Finlayson-Pitts, 2010). The concentrations of these product ions reached a plateau because of the presence of excess isoprene and suppression of the reaction.

The optical properties of the products were more complex compared with those of the dinitrate precursor. For descriptive convenience, we named the reaction pathway with m/z of the iconic product, namely NO230, NO232, and NO248 (products of each reaction step were denoted as NO230S1, NO230S2, NO230S3, NO232S1 NO232S2, and NO230S3), as seen in Fig. 3. The pathway involving the first-generation intermediate (m/z 230) produced three stable products, the light absorption increased with the formation of nitrate, and λ_{max} shifted to 300 nm. With further oxidation, more oxygen atoms were added to the compound. The second- and third-generation oxidation products were relative stable and less active, as seen in Fig. S3. The optical properties low than 200 nm could barely be observed using an anti-vacuum spectrometer (Radziemski et al., 2005). The C5-hydroxynitrate (m/z 232) route had a long reaction chain and formed molecules of large

weight. The absorption decreased in the first generation, increased in the second, and then decreased in the third. The transition energy also decreased, as reflected in the increase in λ_{max}. The λ_{max} of the third-generation products shifted to the visible region (510 nm). The optical property of the NO248 path was stable, and the intensity and shape of the absorption peak remained close to those of isoprene.

The light absorption generally tended to show a bathochromic shift at first and a hyperchromic shift with further oxidation. The change in optical properties originated from the newly formed functional group. The π–π* transition dominated the precursor isoprene, which had strong light absorption in the SUV region. The newly formed chromophore, –ONO$_2$, features an n–π* transition. The auxochromes –OO–, –OH, and –OOH underwent n→σ* excitation upon interaction with light. The various functional groups differed in terms of absorption, and the excitation energies of –OO–, –OH, and –OOH were higher than that of –ONO$_2$. This difference accounted for the lower λ_{max} of the molecules that included more –OO–, –OH, and –OOH groups. Various oxidation products in field studies or laboratory experiments tend to be mixtures (Bates et al., 2016).

3.4. Evaluation of the light absorption variation over the GZB

The absorbance was positively correlated with concentrations when the level was lower than 1 mol (Li, 2002), accordingly, molar absorption coefficient of each molecule can be superimposed on concentration. The oxidation product in the near ground state occurred at trace levels; therefore, the absorbance was positively correlated with the concentration at a unit distance. The spatial distribution of isoprene and oxidation products were simulated using WRF-Chem 3.5.1, and interactive data language was used to visualize the trends.

The reaction pathway was selected according to its occurrence frequency in the atmosphere; β-ISOOOH and β-ISOPOX are the most abundant products in OH-initiated reaction in the atmosphere (Bates et al., 2014). MACR and its correspondent further oxidized SOAs, dominating the O$_3$-initiated reaction. In the NO$_3$/isoprene reaction, 77%–90% of the total RO$_2$ at night is predicted to react with NO$_3$; therefore, the species at m/z 321 and its oxidized correspondent is the main product in ambient conditions (Ng et al., 2008). The spatial distribution of oxydates absorbance in GZB is demonstrated in Fig. S4. The 9-panel figure lists the absorbance of precursor, fist-generations product and deep oxidation products of OH, O$_3$ and NO$_3$. The colors in Fig. S4 represent absorption intensity: the absorbance weakens when the color changes from red to green. Evidently, the light absorption intensity of oxydates decreased and then increased because the functional group changed in the OH oxidation route (Fig. S4 A1-3). In Fig. S4 B1-3, the absorption of ozone oxydates was observed weakened with further oxidation. However, NO$_3$-initiated oxidation produced highly functionalized products with absorption extending to long wavelengths as shown in Fig. S4 C1-3; their broadband absorption extends from 350 nm, which causes the brown appearance. The O$_3$-initiated reactions did not cause a brown carbonization effect, even in the regional scale. Fig. S4 also suggests that the wavelength-specific absorptivity of oxydates for isoprene varied with geographic location. To the south of the GZB is Qinling Mountain, which has dense forest coverage, and therefore, isoprene level near-ground should be high. Its contribution to absorption was much higher than isoprene from the urban vegetation, as can be discerned from the color variation in Fig. S4.

The reaction with OH, O$_3$, and NO$_3$ could lead to changes in the volatility, optical properties, and other physicochemical properties. The second- and higher-generation oxidation products of isoprene are more likely to partition to the condensed phase than the first-generation products are. Combined with their enhanced polarity and hydrophilic properties, the oxidation products significantly affect the climate by affecting the process of CCN formation (Gomez-Hernandez et al., 2016). The light absorption property led to direct radiative forcing of oxidized isoprene, which is another vital pattern that interferes with propagation
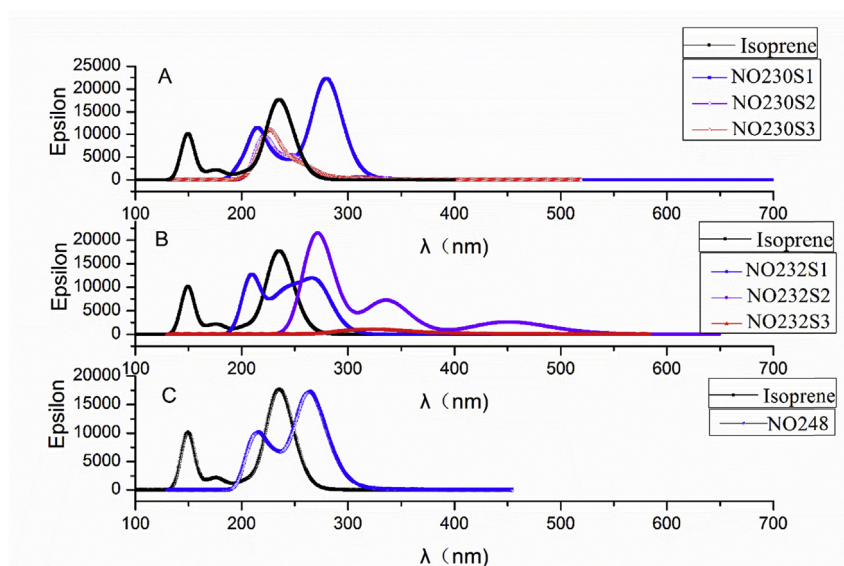
Fig. 3. UV–vis spectrum of the oxydates of isoprene reacted with NO3.

of solar and terrestrial radiation (Shrivastava et al., 2017). Furthermore, convincing evidence pointed to the indispensable role of direct radiative forcing of oxydates for isoprene in climate models (Moise et al., 2015).

The optical properties of products from oxidation with OH, O_3, and NO_3 vastly differed from those of the precursor isoprene. Oxidation products of OH and O_3 were less absorptive, indicating less radiative forcing. The reaction of NO_3 with isoprene was a browning process of organics, with oxidation products showing light absorption at 300–500 nm. Thus, the anthropogenic source of oxidants had a high potential to strengthen radiation forcing at night.

In this study, oxydates of GZB in April 2013 is a case study. The WRF-chem simulation only reflected the trend at that time, and may be not applicable to other seasons. In fact, the levels of OH, O_3, and NO_3 varied seasonally and spatially. Moreover, OH, O_3, NO_3 would compete reaction to some extent (Carlton et al., 2009). For example, OH and O_3 were both active in daytime, but concentration and reactivity of OH is higher than O_3, so OH oxidation is overwhelming at most of the time (Bates et al., 2016). NO_3 oxidation happened during nighttime which enable less possibility to compete with the former two (Horowitz et al., 2007).

4. Conclusion

Isoprene is involved in ambient reactions with OH, O_3, and NO_3, which are oxidants that have high reactivity. Their reactions with isoprene are critical sources of SOAs in the atmosphere. The reaction mechanism under various conditions has been made clear through years of research. The UV–vis light absorptive ability of the products with known reaction pathways were calculated at the PBE1PBE/TZVP level using Gaussian 09; Gaussian 09 is a versatile tool for elucidating the light absorption properties during the transformation of isoprene to a highly oxygenated state. Such a study does not replace actual field experiments, but it provides data obtained with a degree of control that is not possible in the atmosphere. We found that light absorption properties did not show direct dependence on molecular weight. UV–vis light absorption intensity and λ decreased during the reaction of O_3 and OH with isoprene; in addition, the λ_{max} of the product from the NO_3 reaction extended to 300–500 nm, which signified a browning effect. WRF-Chem was used to explain the variation of molecules in the GZB; clearly, the oxidation process changed their optical properties. In conclusion, the optical properties of isoprene during the oxidation process depend on the oxidation pathway because of the change in chromophores. Therefore, this study provides a method for searching appropriate chromophores for BrC and for studying its transformation mechanism. As acidity is one of peripheral factors that would affect the optical properties, the effect of acidity on UV-vis spectrum through charge transfer will be conducted in the near future.

Acknowledgements

Appendix A. Supplementary data

Supplementary data to this article can be found online at https://doi.org/10.1016/j.atmosenv.2018.09.017.

References

Adamo, C., Jacquemin, D., 2013. The calculations of excited-state properties with time-dependent density functional theory. Chem. Soc. Rev. 42, 845–856.

Almandoz, M.C., Sancho, M.I., Duchowicz, P.R., Blanco, S.E., 2014. UV–Vis spectroscopic study and DFT calculation of the solvent effect of trimethoprim in neat solvents and aqueous mixtures. Spectrochim. Acta A 129, 52–60.

Bates, K.H., Crounse, J.D., St Clair, J.M., Bennett, N.B., Nguyen, T.B., Seinfeld, J.H., Stoltz, B.M., Wennberg, P.O., 2014. Gas phase production and loss of isoprene epoxydiols. J. Phys. Chem. 118, 1237–1246.

Bates, K.H., Nguyen, T.B., Teng, A.P., Crounse, J.D., Kjaergaard, H.G., Stoltz, B.M., Seinfeld, J.H., Wennberg, P.O., 2016. Production and fate of C4 dihydroxycarbonyl compounds from isoprene oxidation. J. Phys. Chem. 120, 106–117.

Binkowski, F.S., 2003. Models-3 community Multiscale Air quality (CMAQ) model aerosol component 1. Model description. J. Geophys. Res. 108 (D6), 4183–4201.

Campetella, M., Maschietto, F., Frisch, M.J., Scalmani, G., Ciofini, I., Adamo, C., 2017. Charge transfer excitations in TDDFT: a ghost-hunter index. J. Comput. Chem. 38, 2151–2156.

Campuzanojost, P., Williams, M.B., L D'Ottone, A., Hynes, A.J., 2004. Kinetics and mechanism of the reaction of the hydroxyl radical with h8-isoprene and d8-isoprene: isoprene absorption cross sections, rate coefficients, and the mechanism of hydroperoxyl radical production. J. Phys. Chem. 108 (9), 1537–1551.

Carlton, A.G., Wiedinmyer, C., Kroll, J.H., 2009. A review of secondary organic aerosol (soa) formation from isoprene. Atmos. Chem. Phys. 9 (14), 4987–5005.

Doltsinis, N.L., 2014. Time-dependent Density Functional Theory. Oxford University Press, pp. 135–151.

Dudhia, J., 1989. Numerical study of convection observed during the winter monsoon experiment using a mesoscale two-dimensional model. J. Atmos. Sci. 46, 3077–3107.

Dudhia, J., 1996. A multi-layer soil temperature model for MM5. In: Sixth PSU/NCAR Mesoscale Model Users' Workshop, pp. 1–4.

Ernzerhof, M., Scuseria, G.E., 1999. Assessment of the perdew–burke–ernzerhof exchange-correlation functional. J. Chem. Phys. 110, 5029–5036.

Feng, T., Li, G., Cao, J., Bei, N., Shen, Z., Zhou, W., Liu, S., Zhang, T., Wang, Y., Huang, R.-j., Tie, X., Molina, L.T., 2016. Simulations of organic aerosol concentrations during springtime in the Guanzhong Basin, China. Atmos. Chem. Phys. 16, 10045–10061.

Ghosh, B.N., Topic, F., Sahoo, P.K., Mal, P., Linnera, J., Kalenius, E., Tuononen, H.M., Rissanen, K., 2015. Synthesis, structure and photophysical properties of a highly luminescent terpyridine-diphenylacetylene hybrid fluorophore and its metal complexes. Dalton Trans. 44, 254–267.

Gomez-Hernandez, M., McKeown, M., Secrest, J., Marrero-Ortiz, W., Lavi, A., Rudich, Y., Collins, D.R., Zhang, R., 2016. Hygroscopic characteristics of alkylaminium carboxylate aerosols. Environ. Sci. Technol. 50, 2292–2300.

Guenther, A.B., Jiang, X., Heald, C.L., Sakulyanontvittaya, T., Duhl, T., Emmons, L.K., Wang, X., 2012. The Model of Emissions of Gases and Aerosols from Nature version 2.1 (MEGAN2.1): an extended and updated framework for modeling biogenic emissions. Geosci. Model Dev. (GMD) 5, 1471–1492.

Hong, S., 2006. A new vertical diffusion package with an explicit treatment of entrainment processes. Mon. Weather Rev. 134 (9), 2318.

Hong, S.Y., Lim, J.O.J., 2006. The wrf single-moment 6-class microphysics scheme (wsm6). Asia-Pacific J Atmos Sci 42, 129–151.

Horowitz, L.W., Fiore, A.M., Milly, G.P., Cohen, R.C., Perring, A., Wooldridge, P.J., Hess, P.G., Emmons, L.K., Lamarque, J.-F., 2007. Observational constraints on the chemistry of isoprene nitrates over the eastern United States. J Geophysic Res Atmos 112 (D12), 12–18.

Huang, W., Zhang, X.H., Wang, L.Y., Zhai, G.H., Wen, Z.Y., Zhang, Z.X., 2010. The experimental and theoretical study of crystal structure, IR, 1H NMR and UV–vis of 2-styryl-β-naphthathiazole dye. J. Mol. Struct. 977, 39–44.

Ignatov, S.K., Gadzhiev, O.B., Razuvaev, A.G., Masunov, A.E., Schrems, O., 2014. Adsorption of glyoxal (CHOCHO) and its UV photolysis products on the surface of atmospheric ice nanoparticles. DFT and density functional tight-binding study. J. Phys. Chem. C 118, 7398–7413.

Inomata, S., Sato, K., Hirokawa, J., Sakamoto, Y., Tanimoto, H., Okumura, M., Tohno, S., Imamura, T., 2014. Analysis of secondary organic aerosols from ozonolysis of isoprene by proton transfer reaction mass spectrometry. Atmos. Environ. 97, 397–405.

Kroll, Jesse H., Ng, Nga L., Murphy, Shane M., Flagan, Richard C., Seinfeld, John H., 2006. Secondary organic aerosol formation from isoprene photooxidation. Environ. Sci. Technol. 40 (6), 1869–1877.

Lei, W., Zhang, R., Mcgivern, W.S., Derecskeikovacs, A., North, S.W., 2000. Theoretical study of isomeric branching in the isoprene-OH reaction: implications to final product yields in isoprene oxidation. Chem. Phys. Lett. 326 (1–2), 109–114.

Li, R., 2002. Spectral Analysis of Organic Structures [M]. Tianjin University Press, pp. 91–92.

Li, G., Lei, W., Bei, N., Molina, L.T., 2012. Contribution of garbage burning to chloride and PM2.5 in Mexico City. Atmos. Chem. Phys. 12, 8751–8761.

Lin, Y.H., Zhang, H., Pye, H.O.T., Zhang, Z., Marth, W.J., Park, S., et al., 2013. Epoxide as a precursor to secondary organic aerosol formation from isoprene photooxidation in the presence of nitrogen oxides. Proc. Natl. Acad. Sci. U. S. A. 110 (17), 6718–6723.

Liu, J., Lin, P., Laskin, A., Laskin, J., Kathmann, S.M., Wise, M., Caylor, R., Imholt, F., Selimovic, V., Shilling, J.E., 2016. Optical properties and aging of light-absorbing secondary organic aerosol. Atmos. Chem. Phys. 16, 12815–12827.

Lockwood, A.L., Shepson, P.B., Fiddler, M.N., Alaghmand, M., 2010. Isoprene nitrates: preparation, separation, identification, yields, and atmospheric chemistry. Atmos. Chem. Phys. 10, 6169–6178.

Mlawer, E.J., Taubman, S.J., Brown, P.D., Iacono, M.J., Clough, S.A., 1997. Radiative transfer for inhomogeneous atmospheres: RRTM, a validated correlated-k model for the longwave. J. Geophys. Res. Atmos. 102, 16663–16682.

Mogensen, D., Gierens, R., Crowley, J.N., Keronen, P., Smolander, S., Sogachev, A., Nölscher, A.C., Zhou, L., Kulmala, M., Tang, M.J., Williams, J., Boy, M., 2015. Simulations of atmospheric OH, O3 and NO3 reactivities within and above the boreal forest. Atmos. Chem. Phys. 15, 3909–3932.

Moise, T., Flores, J.M., Rudich, Y., 2015. Optical properties of secondary organic aerosols and their changes by chemical processes. Chem. Rev. 115, 4400–4439.

Newland, M.J., Rickard, A.R., Vereecken, L., Muñoz, A., Ródenas, M., Bloss, W.J., 2015. Atmospheric isoprene ozonolysis: impacts of stabilised Criegee intermediate reactions with SO2, H2O and dimethyl sulfide. Atmos. Chem. Phys. 15, 9521–9536.

Ng, N., Kwan, A., Surratt, J.D., Chan, A., Chhabra, P., Sorooshian, A., Pye, H., Crounse, J., Wennberg, P., Flagan, R., 2008. Secondary organic aerosol (soa) formation from reaction of isoprene with nitrate radicals (NO3). Atmos. Chem. Phys. 8 (14), 2164–2167.

Nguyen, T.B., Tyndall, G.S., Crounse, J.D., Teng, A.P., Bates, K.H., Schwantes, R.H., Coggon, M.M., Zhang, L., Feiner, P., Milller, D.O., Skog, K.M., Rivera-Rios, J.C., Dorris, M., Olson, K.F., Koss, A., Wild, R.J., Brown, S.S., Goldstein, A.H., de Gouw, J.A., Brune, W.H., Keutsch, F.N., Seinfeld, J.H., Wennberg, P.O., 2016. Atmospheric fates of Criegee intermediates in the ozonolysis of isoprene. Phys. Chem. Chem. Phys. 18, 10241–10254.

Ou, Q., Bellchambers, G.D., Furche, F., Subotnik, J.E., 2015. First-order derivative couplings between excited states from adiabatic tddft response theory. J. Chem. Phys. 142 (6) 4549-192.

Paulot, F., Crounse, J.D., Kjaergaard, H.G., Kurten, A., Clair, J.M., Seinfeld, J.H., Wennberg, P.O., 2009. Unexpected epoxide formation in the gas-phase photooxidation of isoprene. Science 325 (5941), 730–733.

Paulson, S.E., Seinfeld, J.H., 1992. Development and evaluation of a photooxidation mechanism for isoprene. J. Geophys. Res. Atmos. 97 (D18), 20703–20715.

Peeters, J., Nguyen, T.L., Vereecken, L., 2009. HOx radical regeneration in the oxidation of isoprene. Phys. Chem. Chem. Phys. 11, 5935–5939.

Peeters, J., Muller, J.F., Stavrakou, T., Nguyen, V.S., 2014. Hydroxyl radical recycling in isoprene oxidation driven by hydrogen bonding and hydrogen tunneling: the upgraded LIM1 mechanism. J. Phys. Chem. 118, 8625–8643.

Radziemski, L., Cremers, D.A., Benelli, K., Khoo, C., Harris, R.D., 2005. Use of the vacuum ultraviolet spectral region for laser-induced breakdown spectroscopy-based Martian geology and exploration. Spectrochim. Acta B Atom Spectrosc. 60 (2), 237–248.

Rollins, A.W., Kiendlerscharr, A., Fry, J., Brauers, T., 2009. Isoprene oxidation by nitrate radical: alkyl nitrate and secondary organic aerosol yields. Atmos. Chem. Phys. 9 (2), 6685–6703.

Schwantes, R.H., Teng, A.P., Nguyen, T.B., Coggon, M.M., Crounse, J.D., St Clair, J.M., Zhang, X., Schilling, K.A., Seinfeld, J.H., Wennberg, P.O., 2015. Isoprene NO3Oxidation products from the RO2 + HO2 pathway. J. Phys. Chem. 119, 10158–10171.

Seibert, J., Bannwarth, C., Grimme, S., 2017. Biomolecular structure information from high-speed quantum mechanical electronic spectra calculation. J. Am. Chem. Soc. 139, 11682–11685.

Shen, Z.X., Zhang, Q., Cao, J.J., Zhang, L.M., Lei, Y.L., Huang, Y., Huang, R.J., Gao, J.J., Zhao, Z.Z., Zhu, C.S., Yin, X.L., Zheng, C.L., Xu, H.M., Liu, S.X., 2017a. Optical properties and possible sources of brown carbon in PM2.5 over Xi'an, China. Atmos. Environ. 150, 322–330.

Shen, Z.X., Lei, Y.L., Zhang, L.M., Zhang, Q., Zeng, Y.L., Tao, J., Zhu, C.S., Cao, J.J., Xu, H.M., Liu, S.X., 2017b. Methanol extracted Brown Carbon in PM2.5 over Xi'an, China: seasonal variation of optical properties and sources identification. Aerosol. Sci. Eng. 1–9.

Shrivastava, M., Cappa, C.D., Fan, J., Goldstein, A.H., Guenther, A.B., Jimenez, J.L., Kuang, C., Laskin, A., Martin, S.T., Ng, N.L., Petaja, T., Pierce, J.R., Rasch, P.J., Roldin, P., Seinfeld, J.H., Shilling, J., Smith, J.N., Thornton, J.A., Volkamer, R., Wang, J., Worsnop, D.R., Zaveri, R.A., Zelenyuk, A., Zhang, Q., 2017. Recent advances in understanding secondary organic aerosol: implications for global climate forcing. Rev. Geophys. 55, 509–559.

Suh, I., Wenfang Lei, A., Zhang, R., 2001. Experimental and theoretical studies of isoprene reaction with no3. J. Phys. Chem. 105 (26), 6471–6478.

Surratt, J.D., Finlayson-Pitts, B.J., 2010. Reactive intermediates revealed in secondary organic aerosol formation from isoprene. Proc. Natl. Acad. Sci. U.S.A. 107 (15), 6640–6645.

Werner, Gerhard, Kastler, Jürgen, Looser, Ralf, Ballschmiter, K., 1999. Organic nitrates of isoprene as atmospheric trace compounds. Angew. Chem. 38, 1634–1637.

Wong, J.P.S., Nenes, A., Weber, R.J., 2017. Changes in light absorptivity of molecular weight separated Brown carbon due to photolytic aging. Environ. Sci. Technol. 51, 8414–8421.

Zhang, X., Lin, Y., Surratt, J.D., Zotter, P., Prévôt, A.S.H., Weber, R.J., 2011. Light-absorbing soluble organic aerosol in los angeles and atlanta: a contrast in secondary organic aerosol. Geophys. Res. Lett. 38 (21), 759–775.